

Rashba spin-orbit interaction in graphene armchair nanoribbons

Lucia Lenz¹, Daniel F. Urban², and Dario Bercioux^{1,3}

¹ Freiburg Institute for Advanced Studies, Albert-Ludwigs-Universität, D-79104 Freiburg, Germany

² Physikalisches Institut, Albert-Ludwigs-Universität, D-79104 Freiburg, Germany

³ Department of Physics, Stanford University, Stanford, California 94305, USA

E-mail: lucia.lenz@frias.uni-freiburg.de

Abstract. We study graphene nanoribbons (GNRs) with armchair edges in the presence of Rashba spin-orbit interaction (RSOI). We impose the boundary conditions on the tight binding Hamiltonians for bulk graphene with RSOI by means of a sine transform and use the results to derive different approximations and to investigate their ranges of validity. Finally, we derive an approximation for the lowest two energy bands, which is valid for experimentally available sizes of RSOI. In addition we study the spin polarization in GNRs resulting from the RSOI.

1. Introduction

Spintronics is a multidisciplinary field whose central theme is the active manipulation of the spin degree-of-freedom in solid state systems [1]. The integration of spintronics concepts into standard electronic devices is an important technological challenge for the semiconductor industry. The goal is the realization of devices, which for equal sizes, have better performance and lower power consumption with respect to state-of-the-art electronic devices [2]. In this respect, graphene has great potential for spintronics applications [3]. On the one hand it is characterized by very weak spin-orbit interactions (SOIs) [4] making pristine graphene the spintronics material with the longest spin-coherence time [5]. On the other hand, there are several promising proposals to manipulate the spin states via local material engineering of the graphene membrane [6, 7].

There are two possible types of SOIs in graphene: intrinsic and Rashba (R). Both of them can be understood in terms of the symmetry properties of the honeycomb lattice [8] and by tight binding arguments [4]. The intrinsic SOI opens a gap in the energy spectrum and transforms graphene into a two-dimensional topological insulator [8]. However, intrinsic SOI is extremely weak in pristine graphene. Armchair GNRs with intrinsic SOI have been studied in reference [9].

The RSOI is mainly connected to the overlap of the π and the σ orbitals of the carbon atoms in the sp^2 -hybridization. It can be manipulated by an electric field perpendicular to the graphene plane or by the local curvature of the graphene sheet [4]. Alternatively, it was proposed that RSOI can be enhanced by modifying the bonding within the graphene sheet by covering it with, *e.g.*, hydrogen [10]. It has been predicted that the first two methods lead to a RSOI strength of $\lambda \sim 1\text{meV}$ while the third method could lead to a RSOI strength of approximately one order of magnitude larger. In an experimental study [7] it was shown that opportune substrate engineering could even lead to $\lambda \sim 200\text{ meV}$. Thus there is quite some reason to hope that manipulation of RSOI in graphene will soon become good enough to realize RSOI based spintronics devices. In this respect several efforts have already been made in order to investigate the spintronics properties of bulk graphene, *e.g.* in the case of inhomogeneous SOI structures [11, 12, 13, 14, 15].

However, particularly interesting for graphene is the stripe geometry, the so-called graphene nanoribbon (GNR). While large graphene sheets are still polycrystalline and far from perfect, GNRs with an armchair edge (cf. figure 1) have already been synthesized with atomic precision and well defined edges [16]. In this case, the dangling σ -bonds of the GNRs were passivated with hydrogen, so that also at the edges the sp^2 -hybridization is preserved.

So far GNRs with RSOI and zig-zag edges have been intensely studied. For example, Zarea and Sandler [17] derived the analytic energy spectrum of a zig-zag GNR with RSOI produced by an electric field perpendicular to the GNR surface. Gosálbez-Martínez *et al.* [18] studied RSOI produced by effects of curvature in zig-zag GNRs. Also GNRs with hardwall boundary conditions and RSOI received some attention [19]. On the contrary, armchair GNRs with RSOI received little attention so far — despite of their experimental availability [16].

In this article, we fill the gap and study armchair GNRs with RSOI using an exact and different approximative methods. The article is organized as follows. Section 2 presents the system studied and reviews the ingredients needed to derive the RSOI Hamiltonian for an armchair GNR in section 3.1. We linearize the nearest-neighbor

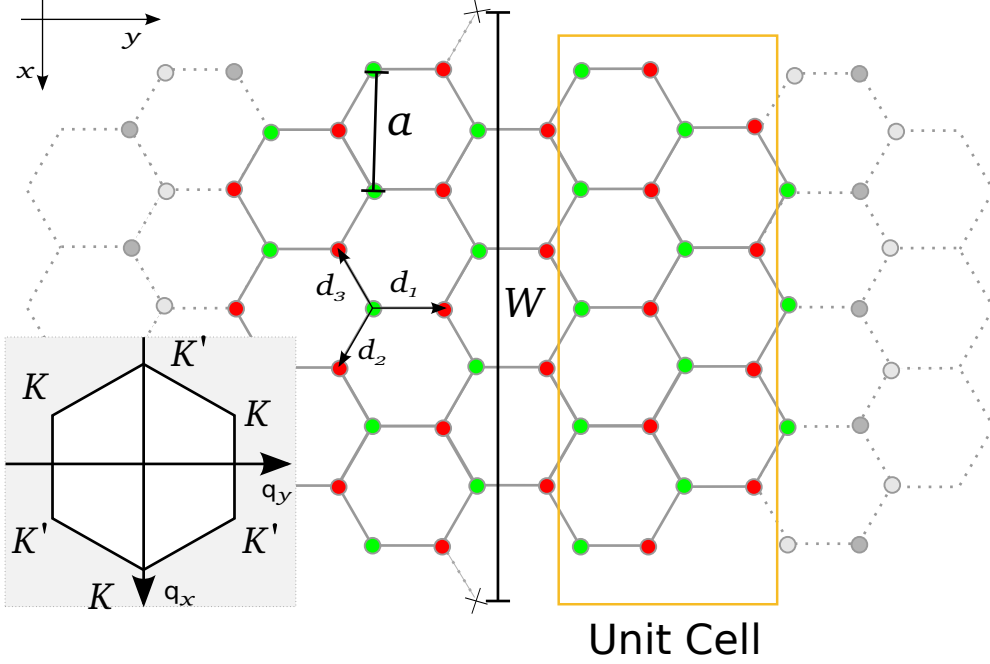


Figure 1. An armchair GNR of width $\bar{W} = 4a$ is shown, where a is the width of the hexagon. The green and red dots mark the A and B atoms of the honeycomb lattice, respectively. Here \mathbf{d}_1 , \mathbf{d}_2 and \mathbf{d}_3 are the displacement vectors connecting nearest neighbor sites. The yellow square indicates the unit cell of the ribbon, with $4 \times 4 + 2$ atoms for the width shown. The distance between the first missing rows of carbon atoms is denoted by $W = \bar{W} + a$. The inset depicts the first Brillouin zone of bulk graphene with the two inequivalent K , K' points.

hopping Hamiltonian and the RSOI Hamiltonian in order to investigate armchair GNRs in the Dirac approximation in section 3.2 and obtain an analytic equation for the lowest energy bands in section 3.3. Finally, in section 3.4 we investigate the spin polarization arising due to the RSOI in the ribbon.

2. Basic Theory

2.1. Graphene armchair nanoribbons

We study armchair GNRs with the edge aligned along the y -direction as depicted in figure 1. Here the two inequivalent carbon atoms A and B are marked by green and red dots, respectively. The three displacement vectors which connect nearest neighbor sites are

$$\mathbf{d}_1 = \frac{a}{\sqrt{3}}(0, 1), \quad \mathbf{d}_{2/3} = \frac{a}{\sqrt{3}}\left(\pm \frac{\sqrt{3}}{2}, -\frac{1}{2}\right), \quad (1)$$

where $a = \sqrt{3}a_{cc}$ is the width of the hexagon and $a_{cc} = 0.142$ nm the carbon-carbon distance. For all plots we choose a_{cc} as our unit of length and formally set $a_{cc} = 1$.

The first Brillouin zone of bulk graphene, which is also a hexagon rotated by $\pi/2$ with respect to the graphene lattice, is shown in the inset of figure 1. The wavevectors

in the x and y direction are q_x and q_y , respectively. There are two inequivalent Dirac points, called K and K' , at which the conduction and valence bands touch and, in the absence of RSOI, disperse in a conical shape. For the expansion of the spectrum around the Dirac points, we will use the two points on the q_x axis, namely $K = (4\pi/(3a), 0) = (K_x, 0)$ and $K' = -K$.

There are four atoms for every column of the ribbon and two additional atoms in order to truncate the ribbon in an armchair configuration. Note that in this article, the distance between the first *missing* atoms W will be used instead of the actual width of the ribbon which is $\tilde{W} = W - a$.

2.2. Tight binding Hamiltonians

The Hamiltonian in the tight binding approximation is the starting point of our treatment. The kinetic nearest-neighbor hopping Hamiltonian is given by [20]

$$\mathcal{H}_{\text{kin}} = -t \sum_{i,j} \sum_{\alpha} [b_{\alpha}^{\dagger}(\mathbf{R}_i + \mathbf{d}_j) a_{\alpha}(\mathbf{R}_i) + \text{H.c.}] \quad (2)$$

with the hopping integral $t \approx 2.7$ eV. The operator $a_{\alpha}(\mathbf{R}_i)$ annihilates a quasiparticle on the A atom at lattice position \mathbf{R}_i and with spin α and $b_{\alpha}^{\dagger}(\mathbf{R}_i + \mathbf{d}_j)$ creates a quasiparticle at the B atom at position $(\mathbf{R}_i + \mathbf{d}_j)$ with spin α . The sum over $j = 1, 2, 3$ takes into account the three displacement vectors.

The RSOI Hamiltonian induced by, *e.g.* an electric field perpendicular to the graphene sheet, is given by [17, 21]

$$\mathcal{H}_{\text{SO}} = i\lambda \sum_{i,j} \sum_{\sigma,\sigma'} b_{\sigma'}^{\dagger}(\mathbf{R}_i + \mathbf{d}_j) \left[(\mathbf{s} \times \hat{\mathbf{d}}_j) \cdot \hat{\mathbf{z}} \right]_{\sigma',\sigma} a_{\sigma}(\mathbf{R}_i) + \text{H.c.} \quad (3)$$

and has the form of a spin-dependent nearest-neighbor hopping with hopping integral λ . Here $\hat{\mathbf{z}}$ is the unit vector in z -direction, \mathbf{s} is the vector of Pauli matrices associated with the spin degree of freedom and $\hat{\mathbf{d}}_j$ are the normalized displacement vectors. The Hamiltonian (3) lifts spin degeneracy, since hopping between the A and B atoms is always accompanied by a spin-flip.

2.3. The Dirac approximation

For the Dirac approximation of the nearest-neighbor hopping Hamiltonian (2) the Fourier transform is taken and expanded close to the Dirac points K and K' . Thus, $q_x = \pm K_x + k_x$ and $k_y = q_y$, where k_x and k_y are small compared to $|K|$ [20]. This leads to

$$\mathcal{H}_{\text{Dirac}} = v_F (\tau_z s_0 \sigma_x k_x - \tau_0 s_0 \sigma_y k_y), \quad (4)$$

where $v_F = (\sqrt{3}at)/2$ is the Fermi velocity, σ_i , s_i and τ_i ($i = x, y, z$) are Pauli matrices representing the A/B-sublattices, the fermionic spin, and the K/K' valley degree of freedom, respectively. The index 0 is used for the unit matrix. Note that $\mathcal{H}_{\text{Dirac}}$ contains two blocks $\mathcal{H}_{\text{Dirac}}^K$ and $\mathcal{H}_{\text{Dirac}}^{K'}$ related by time-reversal symmetry (TRS): $\mathcal{H}_{\text{Dirac}}^K(k_x) = \mathcal{H}_{\text{Dirac}}^{K'}(-k_x)$. This facilitates the calculation of the spectrum for an armchair GNR, as we will show in 2.4.

In order to point out some difficulties that arise when RSOI in the Dirac approximation is considered together with armchair boundary conditions, we give the RSOI Hamiltonian up to zeroth order in the wavevector \mathbf{k} (see [4, 8] and Appendix A):

$$\mathcal{H}_{\text{SO}}^0 = \frac{3\lambda}{2} (\tau_0 \sigma_x s_y - \tau_z \sigma_y s_x). \quad (5)$$

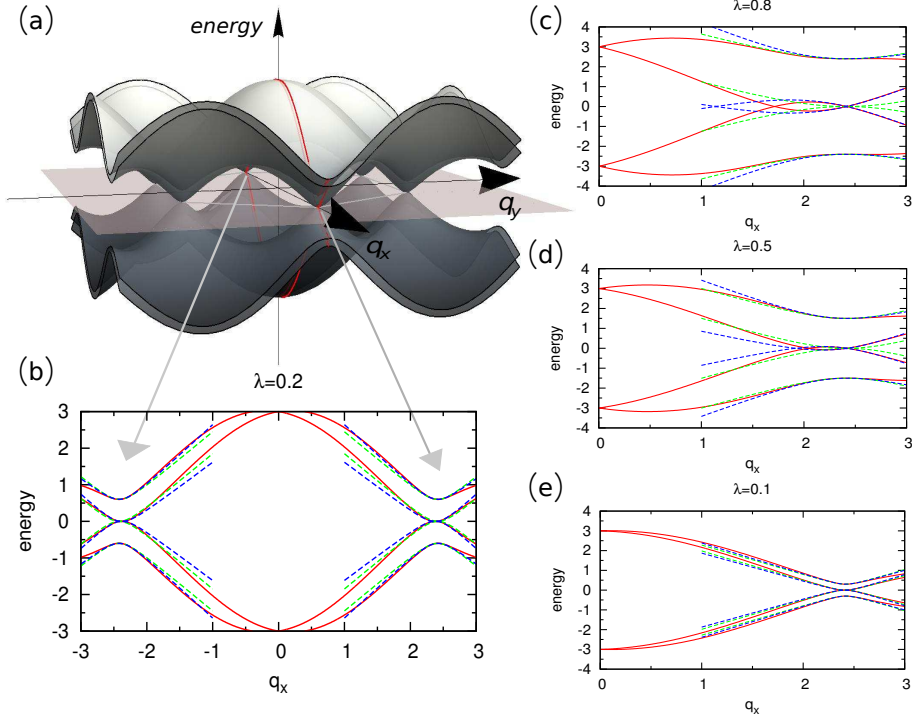


Figure 2. Figure (a) shows the energy dispersion of bulk graphene in the presence of RSOI in dependence of the wavevectors q_x and q_y . The cut along the q_x -axis, marked in red, is shown in figure (b). The blue, dashed line is calculated taking into account \mathcal{H}_{SO} up to first order in k , for the green, dashed line only the zeroth order in k is used for \mathcal{H}_{SO} . Figure (c)-(e) show the same cut for different RSOI strength, λ .

As before, the Hamiltonian obeys TRS. But now it explicitly depends on the spin. Therefore it is impossible to obtain a quantization condition for the wavevectors of a ribbon with RSOI in the low energy approximation, like it is done in section 2.4 for the Dirac Hamiltonian. Therefore, in section 3, we will start from the tight binding Hamiltonians and instead of taking a Fourier transform, we will take a sine transform to ensure that the boundary conditions are fulfilled. Afterwards the linearization can be done without problems.

Before we proceed, let us focus on RSOI in bulk graphene for later comparison. The energy spectrum of bulk graphene for different λ is shown in figure 2. The spectra shown in red are derived from the tight binding Hamiltonians (2) and (3), for the approximations to the spectra shown in light green, the linearized nearest-neighbor hopping Hamiltonian (4) and the zeroth order RSOI Hamiltonian (5) are used. One can see, that the light green spectra do not catch the triangular warping which is observed for $\lambda \approx 0.5t$ and larger. In this case, taking the linear order expansion of the RSOI Hamiltonian (blue, dashed lines) works slightly better. For a derivation of the linear order, see Appendix A or reference [22].

2.4. Armchair boundary conditions for GNRs without RSOI

The boundary conditions for armchair GNRs without RSOI in the Dirac approximation were first studied by Brey and Fertig [23]. We briefly review their results.

The wave function on the graphene lattice for energies close to the Dirac points can be written in terms of slowly varying envelope functions ϕ^K and $\phi^{K'}$. Without taking into account the spin degree of freedom, these functions are two-component spinors and eigenstates of one of the two equivalent upper blocks or one of the two lower blocks of equation (4) in the (a_K, b_K) or $(a_{K'}, b_{K'})$ representation (cf. [Appendix A](#) and reference [20]). The wave function on sub-lattice $\mu = A, B$ can be written as

$$\psi_\mu(x, y) = e^{iK_x x} \phi_\mu^K(x, y) + e^{-iK_x x} \phi_\mu^{K'}(x, y). \quad (6)$$

In this approximation the variables x and y are continuous. The two functions ϕ_μ^K and $\phi_\mu^{K'}$ are expansions of the full wave function at the two different Dirac points K and K' and the fast varying phases $e^{\pm iK_x x}$ are required in order to bring both partial wave functions back into the same coordinate system ($q_x = \pm K + k_x$).

For a ribbon that is cut at $x = 0$ and $x = W$, all wave functions on the missing atoms have to be zero (cf. figure 1). This leads to the boundary conditions

$$\psi_\mu(0, y) = \phi_\mu^K(0, y) + \phi_\mu^{K'}(0, y) = 0, \quad (7)$$

$$\psi_\mu(W, y) = e^{iK_x W} \phi_\mu^K(W, y) + e^{-iK_x W} \phi_\mu^{K'}(W, y) = 0. \quad (8)$$

The boundary condition (7) requires that spinors propagating along the x -axis from the K valley are superimposed with spinors propagating in the opposite direction from the K' valley and *vice versa*, since the corresponding eigenvectors are equal due to TRS. The boundary condition (8) gives the quantization condition on k_x ,

$$k_x^{(n)} \equiv k_n = \pm K_x + \underbrace{\frac{\pi m}{W}}_{q_m} = \frac{n\pi}{W} \pm \frac{4\gamma\pi}{3W}. \quad (9)$$

The integer m labels different transverse *modes* going from $m = 1$ to m_{\max} , which is the total number of modes in a ribbon. The total number of modes, on the other hand, is equal to half the number of atoms in a unit cell, indicated by the yellow square in figure 1. For the second equality sign we rewrite $W = a(3j + \gamma)$ with a positive integer j and $\gamma = -1, 0$ or 1 . The modes n range from $-4j$ to $n_{\max} = m_{\max} - 4j = 4(2j + \gamma) - 2$. The shifted modes n are convenient to work with, because $n = 0$ corresponds to the lowest energy bands. The equation for the energy spectrum of the armchair GNR now reads $E_{n,\epsilon} = \epsilon \sqrt{k_y^2 + k_n^2}$. Only for $\gamma = 0$ the GNR is metallic, since a zero-energy solution is possible for $k_y = 0$. For $\gamma = \pm 1$, the spectrum shows an energy gap equal to $2|q_1| = 2\pi/W$. In the following we will focus on the effect of RSOI on metallic GNRs, though the method employed is general and also applicable if $\gamma \neq 0$.

Finally using the q_m as wavevector the eigenstates of the kinetic Hamiltonian that obey the boundary conditions (7) and (8) are proportional to sine functions,

$$\Psi_{\epsilon,n}(x, y) \propto e^{ik_y y} \Phi_{k_x, k_y, \epsilon}^K \sin(q_m x). \quad (10)$$

Here, $\Phi_{k_x, k_y, \epsilon}^K$ are the two-component eigenvectors of the Dirac Hamiltonian of the K valley, depending on the wavevectors of the exponential ansatz and on the sign of the eigenenergy ϵ . The exact form of these vectors is not needed because we only need to know that the boundary conditions are fulfilled by the sine function (10), to give a physical interpretation to the general sine transform introduced in the next section.

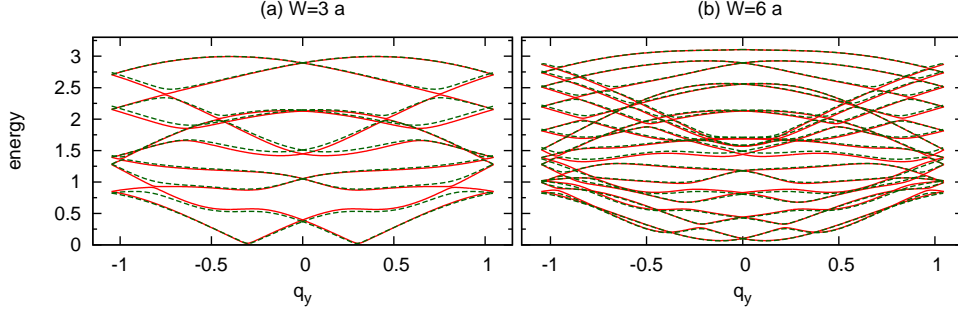


Figure 3. Spectra for two different widths and $\lambda = 0.5t$ are shown. The exact spectra obtained with the sine transform are shown in red. The dark green spectra are calculated using the continuum approximation, equation (16). The two smallest possible widths of metallic GNRs are shown while the spectrum for the same λ and $W = 12a$ can be found in figure 4 (b).

3. Armchair GNRs with RSOI

3.1. Sine transform and continuum limit

It is important to recall here that the tight binding Hamiltonians are expanded over a basis set of counter propagating exponential wave functions to obtain (5) and (4). By definition these states do not fulfill the armchair boundary conditions. For this reason, in order to study the effect of RSOI for the case of an armchair GNR we need to expand the Hamiltonians on a basis set that is naturally fulfilling the boundary condition. Therefore we take the sine transform of the $a_\sigma(\mathbf{R}_i)$ and $b_\sigma(\mathbf{R}_i + \mathbf{d}_j)$ operators in the tight binding Hamiltonians (2) and (3). Taking the sine transform corresponds to choosing a set of basis functions $\propto \sin(q_m x)$ with the mode $q_m = \pi m/W$. We use

$$a_\sigma(\mathbf{R}_i) = \int_{-\infty}^{\infty} dq_y e^{iq_y y_i} \sqrt{\frac{2}{m_{\max}}} \sum_{m=1}^{m_{\max}} \sin(q_m x_i) a_\sigma(q_m, q_y), \quad (11)$$

$$b_\sigma(\mathbf{R}_i + \mathbf{d}_j) = \int_{-\infty}^{\infty} dq_y e^{iq_y (y_i + d_{j,y})} \sqrt{\frac{2}{m_{\max}}} \sum_{m=1}^{m_{\max}} \sin(q_m (x_i + d_{j,x})) \times b_\sigma(q_m, q_y), \quad (12)$$

where $\mathbf{R}_i = (x_i, y_i)$ and $\mathbf{d}_j = (d_{j,x}, d_{j,y})$. The ribbon is assumed to be infinite in y -direction, therefore a continuous wavevector q_y can be used. Inserting the transformation (12) into equation (3) and using $q_m = m\pi/W$ yields

$$\mathcal{H}_{\text{SO}} = \lambda \int dq_y \sum_{m,m'} \sum_{\sigma} \left\{ (\mathcal{A}_{m,m'}^{\text{intra}} + \sigma \mathcal{A}_{m,m'}^{\text{inter}}) b_{-\sigma}^\dagger(q_m, q_y) a_\sigma(q_{m'}, q_y) + [(\mathcal{A}_{m',m}^{\text{intra}})^* + \sigma (\mathcal{A}_{m',m}^{\text{inter}})^*] a_\sigma^\dagger(q_m, q_y) b_{-\sigma}(q_{m'}, q_y) \right\} \quad (13)$$

with

$$\mathcal{A}_{m,m'}^{\text{intra}} = i e^{-iq_y} \left(1 - e^{iq_y/2} \cos(\sqrt{3}q_m/2) \right) \delta_{m,m'}, \quad (14a)$$

$$\mathcal{A}_{m,m'}^{\text{inter}} = \sqrt{3} e^{iq_y/2} \sin(\sqrt{3}q_m/2) \mathcal{B}_{m,m'} \left(\frac{1 - (-1)^{m+m'}}{2} \right), \quad (14b)$$

where $\delta_{m,m'}$ is the Kronecker delta and

$$\mathcal{B}_{m,m'} = \frac{1}{m_{\max} + 1} \left[\cot \left(\frac{\pi(m+m')}{2(m_{\max} + 1)} \right) + \cot \left(\frac{\pi(m-m')}{2(m_{\max} + 1)} \right) \right] \quad (15)$$

We recall that throughout the paper the carbon-carbon-distance a_{cc} is chosen as the unit of length. In the limit of a very wide ribbon we can consider continuous coordinates x and y and use

$$\lim_{m_{\max} \rightarrow \infty} \mathcal{B}_{m,m'} = \frac{4}{\pi} \frac{m'}{(m')^2 - m^2}. \quad (16)$$

There are two terms in the RSOI Hamiltonian: an intra-mode and an inter-mode coupling term. Both couple states with different spin, however, the former is coupling modes with the same mode index $m = m'$, while the latter couples different modes $m \neq m'$ with different parity — i.e. odd modes with even modes. The intra-mode coupling is a peculiarity of GNRs associated to the two inequivalent carbon atoms in the unit cell. No similar effect is present in quantum wires with RSOI [24, 25].

Inserting the transformation (11) and (12) in \mathcal{H}_{kin} , leads to the well known expression:

$$\mathcal{H}_{\text{kin}} = -t \sum_{\sigma} \int_{-\infty}^{\infty} dq_y \sum_{m=1}^{m_{\max}} e^{-iaq_y/\sqrt{3}} \left[1 + 2e^{i\sqrt{3}aq_y/2} \cos \left(\frac{q_m}{2} \right) \right] b_{\sigma}^{\dagger}(q_m, q_y) a_{\sigma}(q_m, q_y) + \text{h.c.}, \quad (17)$$

where, of course, there is no coupling between different modes. The coupling of the two inequivalent valleys K/K' is introduced only by the boundary conditions.

In the figures 3 and 4 the exact spectra are shown in red and the spectra obtained with the continuum approximation (16) in green for different widths and RSOI strengths. In figure 3 the two smallest ribbons are shown with $\lambda = 0.5t$. For the smallest conducting width $W = 3a$ the agreement is not perfect, but for $W = 6a$ the spectrum shows only small deviations for some of the bands. The magnitude of the error introduced by the continuum approximation depends on the value of λ as illustrated in figure 4. The smaller λ , the better the agreement with the continuum approximation, because the case without RSOI has no inter-mode coupling and thus the continuum approximation corresponds to the exact case.

We note in passing that it is remarkable how strongly the shape of the spectra depends on the widths for strong RSOI coupling. We observe three (figure 4 (b)), two (figure 3 (a)) and no Dirac points (figure 3 (b)) for the same $\lambda = 0.5$ and different width. It can even be the case that RSOI opens a gap in the spectrum as in figures 3 (b) and 4 (c).

In the next section we will linearize the Hamiltonians (17) and (13) and investigate for which parameter ranges such a simplified model is valid.

3.2. Linearized \mathcal{H}_{SO} and \mathcal{H}_{kin} for armchair GNR

The linearized version of both the nearest-neighbor hopping Hamiltonian obtained in equation (17) and the RSOI Hamiltonian (13), have the symmetry $\mathcal{H}_{\text{kin/so}}^K(k_n) = \mathcal{H}_{\text{kin/so}}^{K'}(-k_n)$. Therefore we will only give the linearized versions for the K point with k_n and k_y being the small displacements from the K point, i.e. $q_m = K_x + k_n$

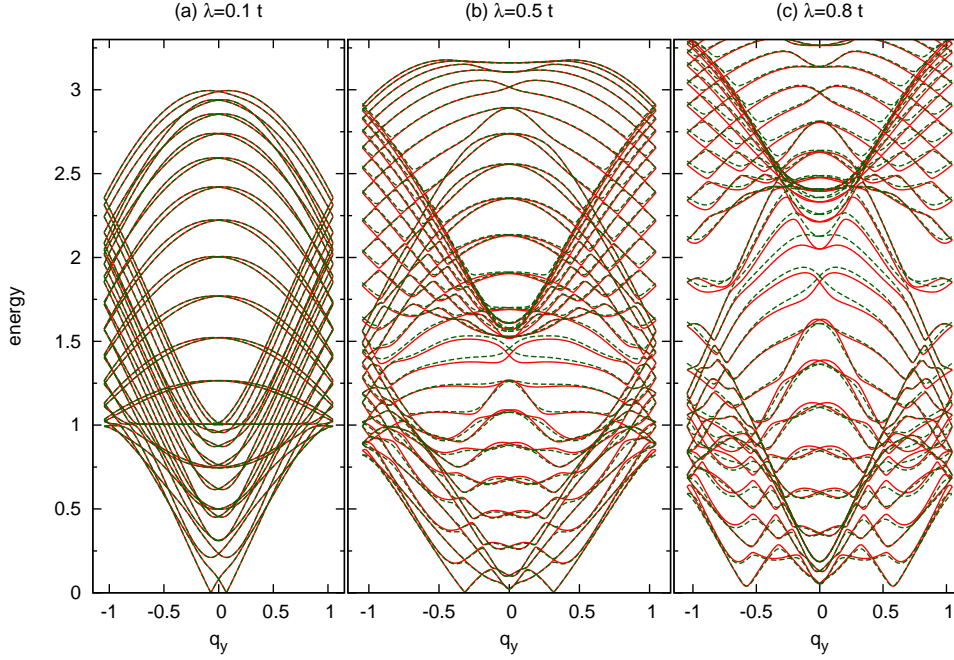


Figure 4. Spectra for different λ and $W = 12a$ are shown. The tight binding results are depicted by full red lines and compared to the continuum approximation using equation (16), depicted by dark green, dashed lines.

and $q_y = K_y + k_y$. A straight forward Taylor series of (17) leads to the well-known Dirac Hamiltonian with quantized wavevector,

$$[\mathcal{H}_{\text{kin}}]_n = v_F s_0 (\sigma_x k_n - \sigma_y k_y), \quad (18)$$

with $\mathcal{H}_{\text{kin}} = \int dq_y \sum_n \psi_n^\dagger [\mathcal{H}_{\text{kin}}]_n \psi_n$ and $\psi_n = \{a_\uparrow(k_n, k_y), b_\uparrow(k_n, k_y), a_\downarrow(k_n, k_y), b_\downarrow(k_n, k_y)\}$. On the other hand, linearizing the coupling matrices (14a) and (14b) around the K-point yields

$$\mathcal{A}_{m,m'}^{\text{intra}} \simeq \delta_{m,m'} \left(\frac{3i}{2} + \frac{3(k_y + ik_m)}{4} \right), \quad (19a)$$

$$\mathcal{A}_{m,m'}^{\text{inter}} \simeq \left(\frac{1 - (-1)^{m+m'}}{2} \right) \frac{3}{\pi(m' - m)} \left(1 + \frac{k_m + k_{m'}}{4} + \frac{ik_y}{2} \right) \quad (19b)$$

Now, the linearized version of the intra-mode RSOI Hamiltonian (13) for modes $n = n'$ reads

$$[\mathcal{H}_{\text{SO}}^{\text{intra}}]_n = \frac{3\lambda}{2} s_x \left(\sigma_y + \frac{\sigma_x k_y + \sigma_y k_n}{2} \right) \quad (20)$$

with $\mathcal{H}_{\text{SO}}^{\text{intra}} = \int dq_y \sum_n \psi_n^\dagger [\mathcal{H}_{\text{SO}}^{\text{intra}}]_n \psi_n$. Comparing the constant terms to the linearized RSOI-Hamiltonian of the infinite graphene plane $\mathcal{H}_{\text{SO}}^0$, cf. equation (5), we observe that this is the same as adding the blocks for the K and the K' valley and dividing by 1/2. This illustrates the coupling of the two valleys induced by the armchair boundary conditions.

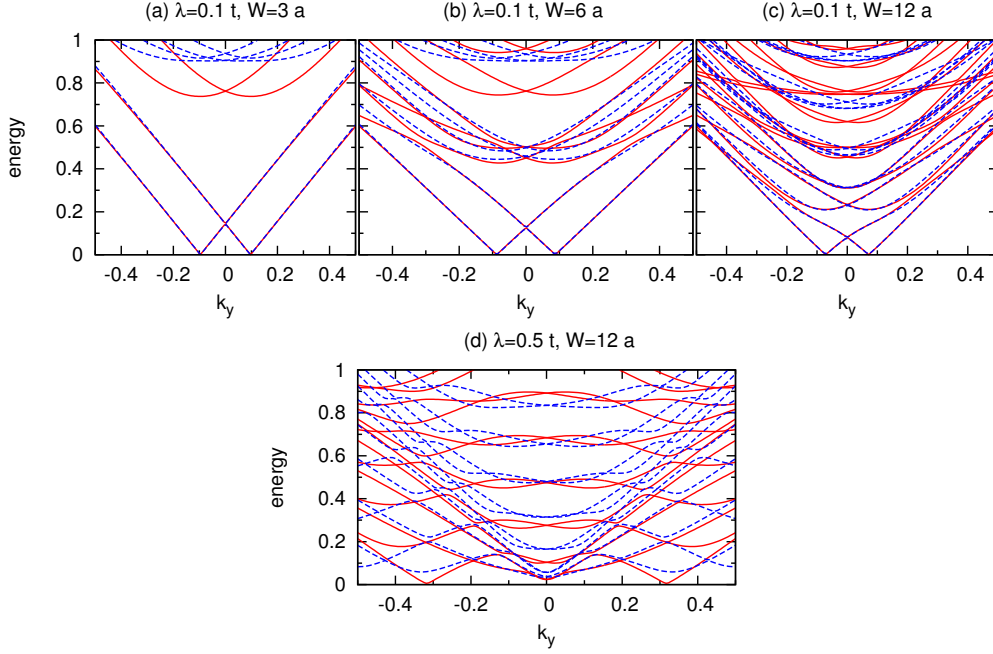


Figure 5. In the upper panel, figure (a)-(c), spectra for different width and $\lambda = 0.1t$ are shown. Figure (d), in the lower panel, shows the spectrum for $\lambda = 0.5t$ and $W = 12a$. The red, full lines depict the exact result while the blue lines show the results after taking the continuum limit and linearizing. The effect of the break down of the continuum approximation is quite pronounced, as shown in figure (a), where only the lowest energy bands agree with the tight binding result. Also for larger ribbons, as shown in figure (b) and (c), the linearization leads to discrepancies. Nevertheless, in figure (c) the bands connected to mode 0 and 1 are already in a good agreement with the tight binding method. For large λ , such as shown in figure (d), the results obtained after linearizing the sine transformed Hamiltonians differ substantially from the tight binding result especially in comparison with figure 4(b)

For small but different $k_n \neq k'_n$ and small k_y the elements of the inter-mode RSOI Hamiltonian are given by

$$[\mathcal{H}_{\text{SO}}^{\text{inter}}]_{n,n'} = \frac{3\lambda(1 - (-1)^{n'+n})}{2\pi i(n' - n)} s_y \left[\sigma_x + \frac{\sigma_y k_y}{2} - \frac{\sigma_x(k_n + k_{n'})}{4} \right] \quad (21)$$

where $\mathcal{H}_{\text{SO}}^{\text{inter}} = \int dq_y \sum_{n,n'} \psi_n^\dagger [\mathcal{H}_{\text{SO}}^{\text{inter}}]_{n,n'} \psi_{n'}$. The main and surprising point about equation (21) is that there is a contribution coupling even and odd bands that does not depend on W but only scales inversely with the distance of the bands.

In figure 5 we show the dependence on the width W for a constant $\lambda = 0.1t$. We have to use smaller λ than in the previous section, since the agreement for $\lambda = 0.5t$ is already quite bad, as shown in figure 5 (d). Although we have not made any additional restriction on λ compared to the preceding section, it is clear from figure 2, which shows spectra for bulk graphene, that, as soon as we come in the regime of triangular warping, the linear approximation to RSOI also catches the behavior only qualitatively. Thus, the linearization is only useful for the low energy and small λ regime. Since up to now only very small RSOI strengths of about a hundredth of t

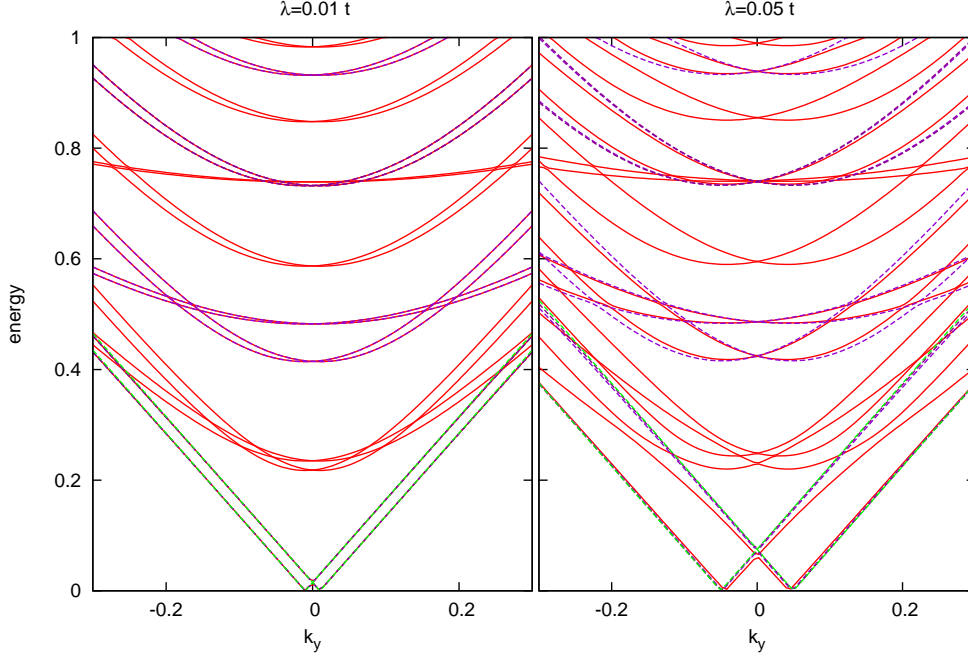


Figure 6. Spectra obtained with equation (22) are shown in light green, together with results of the tight binding method for different width. The red lines correspond to $W = 12a$, the lines colored in magenta correspond to $W = 6a$ and the violet lines to $W = 3a$.

are experimentally available, we will go even further in the next section and derive an analytic approximation for the lowest energy bands only.

3.3. Analytic approximation for the lowest bands

In physical systems the achieved spin-orbit interactions are approximately two orders of magnitude smaller as the hopping integral [7]. Therefore we want to propose a simplified model for the lowest mode bands ($n = 0$). Since the coupling between the bands is as strong as the coupling between spins, which can be seen in equations (21) and (20), and since the band corresponding to $n = 0$ does couple to the bands corresponding to $n = 1$ this model is only valid far away from band crossings. Adding $[\mathcal{H}_{\text{kin}}]_n$ and $[\mathcal{H}_{\text{SO}}^{\text{intra}}]_n$ for $n = 0$ and diagonalizing leads to:

$$E = \pm \frac{3}{2} \sqrt{(k_y \pm \lambda)^2 + \frac{k_y^2 \lambda^2}{2}}, \quad (22)$$

where we have assumed that $t = 1$, $a_{\text{cc}} = 1$. Equation (22) shows that the main correction due to RSOI is the lifting of the spin degeneracy for the $n = 0$ mode bands and a splitting of the Dirac point into two. Furthermore, there is a term proportional to $k_y^2 \lambda^2$, which opens a gap in the spectrum. But since in the current approximation λ and k_y are both small, this term will only have a neglectable effect. Note also, that because we consider the metallic mode ($n = 0$), equation (22) is independent of W . This is demonstrated in figure 6, where equation (22) (light green, dashed

lines) as well as the result of the tight binding method for different W (different tints of red) is shown. For both RSOI strengths that are considered, the low energy behavior is captured reasonably by equation (22), but the figure also indicates that, if $\lambda > 0.05t$, a better approximation, like the one in the preceding section, should be used. Interestingly, for such small λ the width dependence for the modes $n > 0$ only shows up in the dependence of k_n on W . Therefore, for $W = 12a$ the bands corresponding to the modes $n = 0, 1, 2..$ are visible in the energy range shown, while for $W = 6a$ only half the modes are visible and for $W = 3a$ only one quarter. The mode $n = 2$ for $W = 12a$ gives the same bands as the mode $n = 1$ for $W = 6a$. This indicates that the width dependence comes from k_n only, in contrast to, *e.g.* figure 3, where $\lambda = 0.5t$ and where the width affects the spectra strongly.

3.4. Spin polarization

Here, we study the spin polarization, *i.e.*, the expectation value of the x -component of the spin operator for different bands $[\langle S_x = \frac{1}{2}s_z \otimes \sigma_0 \rangle]_n$, as a function of the momentum along the GNR with the tight binding method.

In figures 7 (a) and (b) we show the results for two different values of RSOI, $\lambda \sim 0.01t$ and $\lambda \sim 0.1t$. Similar to the observations for quantum wires in presence of RSOI [24, 25], the spin polarization shows a smooth crossover to the opposite sign when changing q_y from positive to negative values. In the case of the lowest energy band, shown in red ($n = 0$), the crossover is due to a crossing with a band of the next higher mode ($n = 1$), which is lifted by the terms coupling different modes in \mathcal{H}_{SO} . The violet and the magenta bands have the same mode $n = 1$, but still they show a smooth crossover from positive to negative spin polarization, which cannot be directly attributed to avoided band crossings. Indeed, in the case of quantum wires with RSOI [24, 25] it is possible to split the system Hamiltonian in a part with RSOI along the wire direction and another one perpendicular to the first. In this respect, it is possible to interpret the effects of spin polarization as a function of the mode coupling due to the second term. This separation of the Hamiltonian in different subparts is not possible in the case of a Dirac-like Hamiltonian. However, in analogy to the case of quantum wires, we observe that the spin polarization curves do not have a well defined spin quantization axis. For smaller λ the situation is different as then the influence of the higher mode bands is negligible, since the modes are energetically far apart. This is shown in figure 7 (a). The crossing point of the conduction and the valence band does not influence the spin polarization. The plots show a clear polarization around $q_y = 0$ of either $+1/2$ or $-1/2$ until the first anti-crossing with a higher mode band.

4. Summary and discussion

We have studied graphene nanoribbons with armchair boundaries and finite Rashba spin-orbit interaction. The solution of the stationary Schrödinger equation requires the choice of a basis set which fulfills the boundary conditions set by the ribbon geometry. Therefore the momentum representation of the Hamiltonian is obtained from the real space tight binding Hamiltonian via a sine transform, equation (11) and (12), instead of the (standard) Fourier transform. We emphasize that this procedure is quite different from the case of a graphene armchair nanoribbon without RSOI [23]. There the standard approach is to take a basis set consisting of plain waves, which is

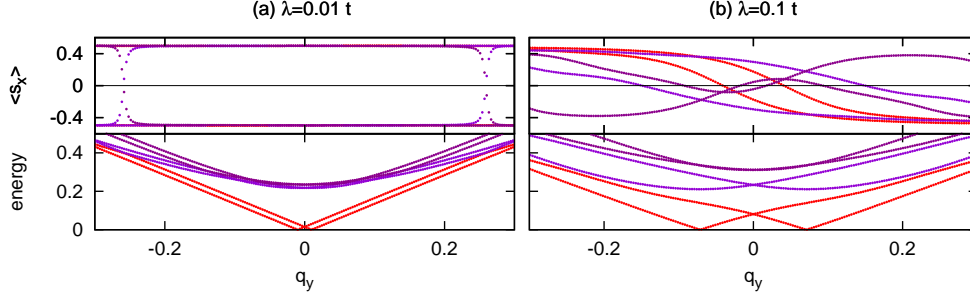


Figure 7. The spin polarization derived from the tight binding approach is shown for (a) $\lambda = 0.001t$ and (b) $\lambda = 0.1t$ and a width of $W = 12a$. In order to compare the energy bands with the spin polarization, in the lower panel the spectra for the two cases are shown in a color coding agreeing with the color coding of the spin polarizations. The lowest mode bands and their polarizations are shown in red, the second lowest bands and their polarizations are shown in violet and the largest shown bands and their polarizations are shown in magenta.

obtained via a Fourier transform of the bulk problem and to take linear combinations of wave function components belonging to the two different K/K' points, cf. equation (10). But the latter basis cannot be used to diagonalize the RSOI part of the Dirac Hamiltonian (5). Due to the derivative operators contained in the expansion up to 1st order in the momentum of the RSOI Hamiltonian, the use of this standard basis is inconsistent and leads to non-Hermitian matrices.

On the other hand, the boundary conditions are naturally satisfied when using the sine transform. We have derived the RSOI Hamiltonian in momentum space which allows to study the effects of finite RSOI on the energy spectrum in a mode dependent manner. Further analytical approximations were presented for the lowest bands and the case of small RSOI. We have analyzed the spectra for a variety of ribbon widths and RSOI strengths. The main effect is that the spin degeneracy is lifted. For large RSOI the spectrum is strongly influenced by the width of the ribbon, while for small RSOI this is not the case. The presence of RSOI can lead to the opening of a gap or to the appearance of a additional Dirac point.

Acknowledgments

The work of LL and DB is supported by the Excellence Initiative of the German Federal and State Governments and the DFG grant BE 4564/1-1. We thank Hermann Grabert and Piet Schijven for fruitful discussions.

Appendix A. Long wave length expansion of the RSOI Hamiltonian

The Rashba Hamiltonian in its tight binding representation was presented in (3). We use the Fourier transformation of the operators

$$a_{\sigma}(\mathbf{R}_i) = \int d^2\mathbf{q} a_{\sigma}(\mathbf{q}) e^{i\mathbf{q} \cdot \mathbf{R}_i} \quad (\text{A.1})$$

$$b_{\sigma}^{\dagger}(\mathbf{R}_i + \mathbf{d}_j) = \int d^2\mathbf{q} b_{\sigma}^{\dagger}(\mathbf{q}) e^{-i\mathbf{q} \cdot (\mathbf{R}_i + \mathbf{d}_j)} \quad (\text{A.2})$$

and the relation

$$(\mathbf{s} \times \hat{\mathbf{d}}_j) \cdot \hat{\mathbf{z}} = s_x d_{y,j} - s_y d_{x,j} = \begin{pmatrix} 0 & d_{y,j} + i d_{x,j} \\ d_{y,j} - i d_{x,j} & 0 \end{pmatrix} \quad (\text{A.3})$$

to write \mathcal{H}_{SO} as:

$$\mathcal{H}_{\text{SO}} = i\lambda \int d^2\mathbf{q} \sum_{\sigma} (d_{y,j} - i\sigma d_{x,j}) e^{-i\mathbf{q}\mathbf{d}_j} b_{-\sigma}^{\dagger}(\mathbf{q}) a_{\sigma}(\mathbf{q}) + \text{H.c.} \quad (\text{A.4})$$

where $\sigma = \uparrow\downarrow = + -$. We use the explicit expressions (1) for the lattice vectors \mathbf{d}_j and after some algebra obtain

$$\mathcal{H}_{\text{SO}} = i\lambda \int d^2\mathbf{q} \sum_{\sigma} b_{-\sigma}^{\dagger}(\mathbf{q}) a_{\sigma}(\mathbf{q}) \times e^{-i\frac{\sigma}{\sqrt{3}}q_y} \left(2 \cos(aq_x/2 + \sigma 2\pi/3) e^{i\frac{\sqrt{3}a}{2}q_y} + 1 \right) + \text{H.c.} \quad (\text{A.5})$$

This is the RSOI Hamiltonian as derived in reference [17]. In order to obtain a low energy approximation we expand around the K and K' points. The Taylor expansion up to first order around the K point ($q_x = k_x - K_x$ and $q_y = k_y$) with $a_{cc} = 1$ gives

$$\begin{aligned} \mathcal{H}_{\text{SO}}^K &\approx \lambda \int d^2\mathbf{k} \left\{ \left[\frac{3}{2} (ik_x + k_y) b_{\downarrow}^{\dagger}(\mathbf{k} + \mathbf{K}) a_{\uparrow}(\mathbf{k} + \mathbf{K}) + \text{H.c.} \right] + \right. \\ &\quad \left. \left[-3ia_{\downarrow}^{\dagger}(\mathbf{k} + \mathbf{K}) b_{\uparrow}(\mathbf{k} + \mathbf{K}) + \text{H.c.} \right] + \mathcal{O}^2(\mathbf{k} - \mathbf{K}) \right\}. \end{aligned} \quad (\text{A.6})$$

At the K' point ($k_x = q_x - K'_x$ and $k_y = q_y$) we obtain in a similar fashion:

$$\begin{aligned} \mathcal{H}_{\text{SO}}^{K'} &\approx \lambda \int d^2\mathbf{k} \left\{ \left[\frac{3}{2} (-ik_x + k_y) b_{\uparrow}^{\dagger}(\mathbf{k} + \mathbf{K}') a_{\downarrow}(\mathbf{k} + \mathbf{K}') + \text{H.c.} \right] + \right. \\ &\quad \left. \left[(-3i) a_{\uparrow}^{\dagger}(\mathbf{k} + \mathbf{K}') b_{\downarrow}(\mathbf{k} + \mathbf{K}') + \text{H.c.} \right] + \mathcal{O}^2(\mathbf{k} - \mathbf{K}') \right\}. \end{aligned} \quad (\text{A.7})$$

References

- [1] I. Zutic, J. Fabian, and S. das Sarma. Spintronics: Fundamentals and applications. *Review Modern Physics* 76:323, April 2004.
- [2] D. D. Awschalom and M. E. Flatte. Challenges for semiconductor spintronics. *Nature Physics* 3:153, March 2007.
- [3] D. Pesin and A. H. MacDonald. Spintronics and pseudospintronics in graphene and topological insulators. *Nature Materials* 11:409, April 2012.
- [4] D. Huertas-Hernando, F. Guinea, and A. Brataas. Spin-orbit coupling in curved graphene, fullerenes, nanotubes, and nanotube caps. *Physical Review B*, 74(15):155426, October 2006.
- [5] N. Tombros, C. Jozsa, M. Popinciuc, H. T. Jonkman, and B. J. van Wees. Electronic spin transport and spin precession in single graphene layers at room temperature. *Nature* 448:571, August 2007.
- [6] C. Weeks, J. Hu, J. Alicea, M. Franz, and R. Wu. Engineering a Robust Quantum Spin Hall State in Graphene via Adatom Deposition. *Physical Review X*, 1:021001 October 2011.
- [7] J. Sánchez-Barriga, A. Varykhalov, M. R. Scholz, O. Rader, D. Marchenko, A. Rybkin, A. M. Shikin, and E. Vescovo. Chemical vapour deposition of graphene on Ni(111) and Co(0001) and intercalation with Au to study Dirac-cone formation and Rashba splitting. *Diamond and Related Materials*, 19:734–741, July 2010.
- [8] C. L. Kane and E. J. Mele. Quantum Spin Hall Effect in Graphene. *Physical Review Letters*, 95(22):226801, November 2005.

- [9] M. Zarea and N. Sandler. Electron-Electron and Spin-Orbit Interactions in Armchair Graphene Ribbons. *Physical Review Letters*, 99, 256804, 2007.
- [10] A. H. Castro Neto and F. Guinea. Impurity-Induced Spin-Orbit Coupling in Graphene. *Physical Review Letters*, 103(2):026804, July 2009.
- [11] D. Bercioux and A. de Martino. Spin-resolved scattering through spin-orbit nanostructures in graphene. *Physical Review B*, 81:165410, April 2010.
- [12] C. Bai, J. Wang, S. Jia, and Y. Yang. Spin-orbit interaction effects on magnetoresistance in graphene-based ferromagnetic double junctions. *Applied Physics Letters* 96:223102, June 2010.
- [13] L. Lenz and D. Bercioux. Dirac-Weyl electrons in a periodic spin-orbit potential. *EPL* 96:27006, August 2011.
- [14] D. Bercioux, D.F. Urban, F. Romeo, and R. Citro. Rashba spin-orbit-interaction-based quantum pump in graphene. *Appl. Phys. Lett.* 101, 122445 (2012).
- [15] M.-H. Liu, J. Bundesmann, and K. Richter. Spin-dependent Klein tunneling in graphene: Role of Rashba spin-orbit coupling. *Physical Review B*, 85(8):085406, February 2012.
- [16] J. Cai, P. Ruffieux, R. Jaafar, M. Bieri, T. Braun, S. Blankenburg, M. Muoth, A. P. Seitsonen, M. Saleh, X. Feng, K. Müllen, and R. Fasel. Atomically precise bottom-up fabrication of graphene nanoribbons. *Nature*, 466:470–473, July 2010.
- [17] M. Zarea and N. Sandler. Rashba spin-orbit interaction in graphene and zigzag nanoribbons. *Physical Review B*, 79(16):165442–+, April 2009.
- [18] D. Gosálbez-Martínez, J. J. Palacios, and J. Fernández-Rossier. Spin-orbit interaction in curved graphene ribbons. *Physical Review B*, 83(11):115436, March 2011.
- [19] T. Stauber and J. Schliemann. Electronic properties of graphene and graphene nanoribbons with ‘pseudo-Rashba’ spin-orbit coupling. *New Journal of Physics*, 11(11):115003, November 2009.
- [20] A. H. Castro Neto, F. Guinea, N. M. R. Peres, K. S. Novoselov, and A. K. Geim. The electronic properties of graphene. *Reviews of Modern Physics*, 81:109–162, January 2009.
- [21] A. de Martino, R. Egger, K. Hallberg, and C. A. Balseiro. Spin-Orbit Coupling and Electron Spin Resonance Theory for Carbon Nanotubes. *Physical Review Letters*, 88(20):206402, May 2002.
- [22] P. Rakyta, A. Kormányos, and J. Cserti. Trigonal warping and anisotropic band splitting in monolayer graphene due to Rashba spin-orbit coupling. *Physical Review B*, 82(11):113405, September 2010.
- [23] L. Brey and H. A. Fertig. Electronic states of graphene nanoribbons studied with the Dirac equation. *Physical Review B*, 73(23):235411, June 2006.
- [24] C.A. Perroni, D. Bercioux, V. M. Ramaglia, and V. Cataudella. Rashba quantum wire: exact solution and ballistic transport. *Journal of Physics: Condensed Matter*, 19:186227, April 2007.
- [25] M. Governale and U. Zülicke. Spin accumulation in quantum wires with strong Rashba spin-orbit coupling. *Physical Review B*, 66(7):073311, August 2002.